Medical Physics
The International Journal of Medical Physics Research and Practice

Real-time ultrasound-tagging to track the 2D motion of the common carotid artery wall in vivo

Guillaume Zahnd, Sébastien Salles, Hervé Liebgott, Didier Vray, André Sérusclat, and Philippe Moulin

Citation: Medical Physics **42**, 820 (2015); doi: 10.1118/1.4905376
View online: http://dx.doi.org/10.1118/1.4905376
View Table of Contents: http://scitation.aip.org/content/aapm/journal/medphys/42/2?ver=pdfcov
Published by the American Association of Physicists in Medicine

Real-time ultrasound-tagging to track the 2D motion of the common carotid artery wall *in vivo*

Guillaume Zahnd[a)]
Biomedical Imaging Group Rotterdam, Departments of Radiology and Medical Informatics, Erasmus MC, Rotterdam 3000 CA, The Netherlands

Sébastien Salles, Hervé Liebgott, and Didier Vray
Université de Lyon, CREATIS, CNRS UMR 5220, INSERM U1044, INSA-Lyon, Université Lyon 1, Lyon 69100, France

André Sérusclat
Department of Radiology, Louis Pradel Hospital, Lyon 69500, France

Philippe Moulin
Department of Endocrinology, Louis Pradel Hospital, Hospices Civils de Lyon, Université Lyon 1, Lyon 69100, France and INSERM UMR 1060, Lyon 69500, France

(Received 17 June 2014; revised 15 December 2014; accepted for publication 21 December 2014; published 21 January 2015)

Purpose: Tracking the motion of biological tissues represents an important issue in the field of medical ultrasound imaging. However, the longitudinal component of the motion (i.e., perpendicular to the beam axis) remains more challenging to extract due to the rather coarse resolution cell of ultrasound scanners along this direction. The aim of this study is to introduce a real-time beamforming strategy dedicated to acquire tagged images featuring a distinct pattern in the objective to ease the tracking.
Methods: Under the conditions of the Fraunhofer approximation, a specific apodization function was applied to the received raw channel data, in real-time during image acquisition, in order to introduce a periodic oscillations pattern along the longitudinal direction of the radio frequency signal. Analytic signals were then extracted from the tagged images, and subpixel motion tracking of the intima–media complex was subsequently performed offline, by means of a previously introduced bidimensional analytic phase-based estimator.
Results: The authors' framework was applied *in vivo* on the common carotid artery from 20 young healthy volunteers and 6 elderly patients with high atherosclerosis risk. Cine-loops of tagged images were acquired during three cardiac cycles. Evaluated against reference trajectories manually generated by three experienced analysts, the mean absolute tracking error was 98 ± 84 μm and 55 ± 44 μm in the longitudinal and axial directions, respectively. These errors corresponded to $28\% \pm 23\%$ and $13\% \pm 9\%$ of the longitudinal and axial amplitude of the assessed motion, respectively.
Conclusions: The proposed framework enables tagged ultrasound images of *in vivo* tissues to be acquired in real-time. Such unconventional beamforming strategy contributes to improve tracking accuracy and could potentially benefit to the interpretation and diagnosis of biomedical images.
 [http://dx.doi.org/10.1118/1.4905376]

Key words: ultrasound-tagging, transverse oscillations, unconventional beamforming, common carotid artery, phase-based motion tracking

1. INTRODUCTION

1.A. Clinical context

Cardiovascular diseases represent the leading cause of human mortality and morbidity.[1] Since arterial stiffness is an independent predictor of cardiovascular events,[2] this index is widely investigated to assess cardiovascular risk. Among the principal risk markers that are generally used to directly quantify arterial stiffness are the pulse wave velocity (PWV), the cross-sectional distensibility, and the ankle–arm index. Other surrogate markers, such as the total coronary calcium score, can also be used to indirectly measure arterial stiffness. Furthermore, intima–media thickness (IMT) provides information about the anatomical modifications of the vessel as the wall progressively thickens during the atherosclerosis process. Yet, cardiovascular risk prediction is a particularly challenging task, and the screening potential of all these traditional risk markers remains limited.[3] Therefore, there is a strong clinical need for novel biomarkers to improve cardiovascular risk prediction.

During the last decade, a novel pathophysiological phenomenon was observed in the common carotid artery (CCA) using B-mode ultrasound (US) imaging.[4] Namely, the wall tissues were indeed reported to undergo a cyclic shearing deformation along the direction parallel to the blood flow. More specifically, this shearing corresponds to the distinct

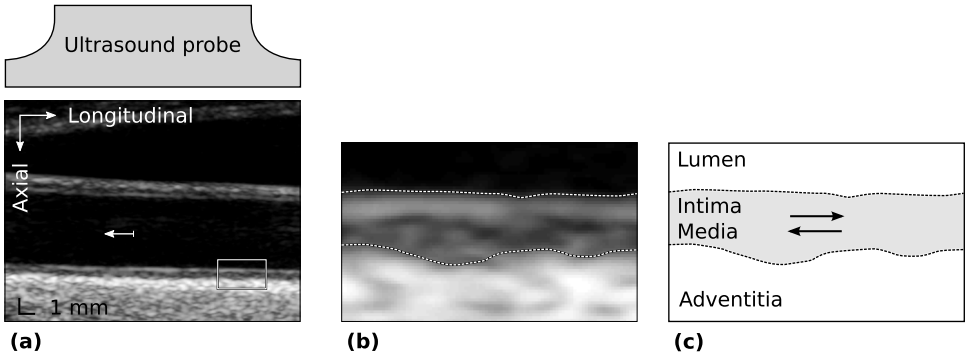

FIG. 1. Structure of the CCA. (a) Longitudinal B-mode ultrasound image of the CCA *in vivo*. The direction of the blood flow is represented by the white arrow. (b) Detailed region of the far wall, corresponding to the rectangle in (a). The lumen–intima and media–adventitia interfaces are indicated by the dotted lines. (c) Schematic representation of the LOKI, represented by the black arrows, corresponding to the cyclic shearing motion of the intima–media complex over the tunica adventitia.

and reproducible longitudinal motion of the intima–media complex over the adventitia layer during the cardiac cycle,[5,6] as displayed in Fig. 1. This phenomenon, hereafter referred to as "*longitudinal kinetics*" (LOKI), was demonstrated by several studies to be associated with the presence of cardiovascular risk factors[7–10] and to predict 1-yr cardiovascular outcome in patients with suspected coronary artery disease.[11] These findings reveal previously unknown mechanisms in the circulatory system and indicate that LOKI could constitute a novel, reliable, and complementary image-based biomarker for cardiovascular risk prediction.

1.B. Limitations of the traditional tracking methods

A number of motion estimation techniques have been proposed to track the motion of the intima–media complex during the cardiac cycle and assess LOKI in B-mode US image sequences (cine-loops), based on speckle tracking,[12] echo-tracking,[13] Kalman filtering,[14] and finite impulse response filtering.[15] Approaches based on raw radio frequency (RF) data have also been proposed to assess LOKI in the CCA.[6,16] However, all these techniques are hindered by an issue inherent to conventional US imaging, namely, the rather coarse resolution cell of the scanner along the longitudinal direction (i.e., perpendicular to the beam axis) w.r.t. the axial direction (i.e., parallel to the beam axis). This phenomenon, due to the characteristics of the scanner's point spread function (PSF), yields the so-called aperture problem, i.e., the perceived longitudinal component of the motion is likely to differ from the actual one. Moreover, the longitudinal profile of the tissues is rather homogeneous since the anatomical layers are aligned along the longitudinal axis and do not present any significant landmark (Fig. 1). For these reasons, the longitudinal component of the wall motion is particularly challenging to extract in conventional US imaging. Therefore, a different approach is required to tackle the challenge of accurate LOKI assessment.

1.C. Phase-based motion estimation

Traditional methods usually rely on spatial information to assess the motion in US imaging, namely, processing is performed directly on pixel intensity values. Conversely, phase-based approaches consist in processing the information carried by the phase of the images, namely, in the frequency domain. Various phase-based motion estimators have indeed been proposed by a large body of literature. An original approach based on the spectral phase using an iterative RF echo phase matching method has been introduced in Ref. 17. A one-dimensional (1D) phase zero-crossing technique was first presented in Ref. 18, and later extended in two dimensions (2D) with the introduction of a synthetic longitudinal phase.[19] A compounding method, based on dual magnitude and phase information, was proposed in Ref. 20. This technique was later applied by the same team to estimate both tissue and flow motions.[21] More recently, monogenic phase has also been exploited in medical US imaging to estimate the motion in 2D (Refs. 22 and 23) as well as in three dimensions (3D).[24,25] Nevertheless, all these phase-based methods are suboptimal, as they are limited by the phase information that is natively embedded in conventional US images. More specifically, the carrier frequency along the axial direction (i.e., parallel to the beam axis) corresponds to the central frequency of the probe, whereas frequencies along the longitudinal direction (i.e., perpendicular to the beam axis) do not abide to any specific pattern.

To cope with the lack of a carrier frequency along the longitudinal direction, specific image formation techniques have been proposed. Such approaches, also called "*beamforming strategies*," consist in applying a controlled scheme to the probe directly during image acquisition, in order to introduce a native longitudinal carrier frequency within the RF signal. A seminal framework has been introduced in the late 1990s and applied to estimate blood velocity from 2D phase signals.[26,27] This technique relies on the production of a pressure field featuring a distinct carrier frequency in both axial and longitudinal directions. This approach is typically achieved using a specific beamforming scheme that consists in the transmission of a plane wave, followed by the reception of backscattered echoes with a dynamic quadratic focusing combined to dynamic apodization. Since the rationale of this framework is to produce a distinct 2D pattern within the images to ease the tracking in US images, it is denoted "*US-tagging*," in reference to the principle

of magnetic resonance imaging tagging (MRI-tagging). A detailed description of this imaging technique is provided later in Sec. 2.A. The terminology "*RF-2D images*" is used to refer to the specific type of tagged-images (i.e., images that feature oscillations along both spatial directions) that are acquired. The denomination "*transverse oscillations*" (TOs) is adopted to define the oscillation pattern that is introduced via the beamforming strategy to modulate the RF signal along the direction perpendicular to the beam axis and produce RF-2D images.

A variety of methods based on US-tagging have been proposed to address multiple applications in medical imaging. In the field of blood flow estimation, several studies have presented improved techniques to assess velocity vectors.[28–31] An implementation on a commercial scanner has also been proposed.[32] Furthermore, US-tagging has been extended to 3D in recent *in silico* studies for vector flow estimation[33] and 3D tissue motion.[34] In elastography, the use of US-tagging has been investigated to enhance the estimation of local tissue deformation.[35–38] As for echocardiography, recent studies have presented an extension of the US-tagging framework to assess the 2D motion of the heart wall[39,40] as well as its deformation.[41] Other studies proposed to exploit the monogenic phase of RF-2D images[42,43] and to adapt TOs beamforming to sector scans performed using a phased array[44] as well as a convex array.[45] The application of US-tagging to assess LOKI in the CCA has also been investigated by our team in a preliminary one-case study,[46] as well as in combination with ultrafast imaging.[47] Accordingly, the introduction of TOs within the images is likely to constitute a major asset to improve the estimation of the longitudinal component of the wall motion.

1.D. Objective and summary of the proposed approach

The aim of the present study is twofold. First, the implementation of an unconventional beamforming strategy on a US research scanner is introduced. This strategy is dedicated to acquire native RF-2D images (i.e., RF images featuring TOs) in real-time (i.e., postprocessing reconstruction of the signals is not required). Second, a motion tracking scheme relying on local phase-based optical flow (LPBOF) is described. This method, previously validated in an *in vitro* phantom pilot study,[46] is devised to extract the trajectory of a single point through the entire length of the cine-loop, via the successive assessment of the motion between pairs of consecutive RF-2D images. The rationale of this two-steps framework lies in the generation and tracking of a specific longitudinal pattern, in the objective to assess more accurately the longitudinal component of the wall motion. Extending preliminary work realized by our team,[34,46,47] the main novelties of the present study are (i) real-time implementation on a scanner for acquisition of actual US-tagged images (as opposed to numerical simulations); (ii) design of a well-suited approximation of the apodization function (described in Sec. 2.B.1); (iii) simultaneous acquisition of a matched series of B-mode images to generate a reference motion via manual tracings from three expert analysts (described in Sec. 2.B.2); and (iv) *in vivo* application and validation on 20 young healthy volunteers as well as 6 elderly patients, in order to determine whether US-tagging may improve LOKI evaluation.

2. MATERIAL AND METHODS

2.A. RF-2D image acquisition via unconventional beamforming strategy

US images are fully characterized by the impulse response of the system, corresponding to the PSF, namely, the echo received when imaging a single scatterer. Therefore, a TOs-featuring PSF yields the generation of RF-2D images. Such a specific PSF, with periodic oscillations in both spatial directions, is typically modeled by a separable 2D function $\mathbf{h}(x,y)$,[48] according to

$$\mathbf{h}(x,y) = \omega(x,y) \cdot \cos\left(\frac{2\pi x}{\lambda_x}\right) \cdot \cos\left(\frac{2\pi y}{\lambda_y}\right), \tag{1}$$

with x and y the longitudinal and axial directions of the image, respectively, λ_x and λ_y the spatial wavelengths corresponding to the oscillations in both spatial directions, and $\omega(x,y)$ a separable 2D Gaussian envelope.

One should notice that in conventional RF images, axial oscillations are natively featured by the PSF, and correspond to the central frequency f_y of the transducer, according to the relation $\lambda_y = c \cdot {f_y}^{-1}$, with c the velocity of the wave propagation in the considered medium. On the other hand, a specific beamforming is required to produce oscillations along the longitudinal profile. In this aim, we propose to control the PSF with a previously developed beamforming strategy.[35,49] This strategy, involving a transmission (TX) phase followed by a reception (RX) phase, can be summarized as follows. The TX phase consists in emitting a broad plane wave, which is supposed to have little influence on the PSF. The RX phase consists in applying a specific aperture function (i.e., dynamic quadratic focusing and apodization) onto the received signal, in order to fulfill the condition of Fraunhofer approximation.[50] The latter states that the beam pattern obtained from a given aperture function can be approximated by the Fourier transform of this aperture function, scaled relatively to the distance from the aperture.

We use this relation to determine, given the characteristics of the desired TOs-featuring PSF, the specific aperture function that requires to be implemented in the RX phase. Using the separable 2D function given by Eq. (1), the longitudinal profile $\mathbf{h}(x)$ of the PSF corresponds to [Fig. 2(a)]

$$\mathbf{h}(x) = e^{-\pi(x/\sigma_x)^2} \cdot \cos\left(\frac{2\pi x}{\lambda_x}\right), \tag{2}$$

with σ_x the full width at half-maximum (FWHM) of the Gaussian envelope $\omega(x)$.

Therefore, by exploiting the Fraunhofer approximation, the corresponding aperture function $\mathbf{w}(x_i)$ applied in RX phase to

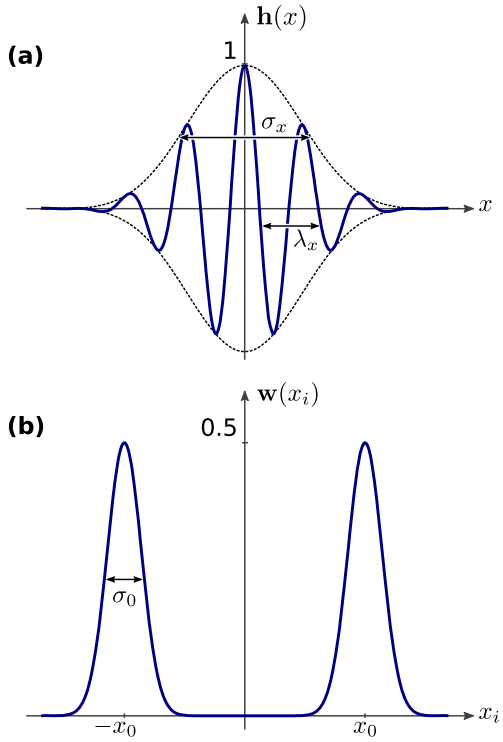

FIG. 2. Unconventional beamforming strategy yielding RF-2D images. (a) Longitudinal profile $\mathbf{h}(x)$ of the PSF, featuring TOs. (b) Specific aperture function $\mathbf{w}(x_i)$, applied onto the elements x_i of the probe in the reception phase. According to the Fraunhofer approximation, $\mathbf{h}(x)$ corresponds to the Fourier transform of $\mathbf{w}(x_i)$.

the ith element x_i of the transducer can be formulated as

$$\mathbf{w}(x_i) = e^{-\pi\left(\frac{x_i - x_0}{\sigma_0}\right)^2} + e^{-\pi\left(\frac{x_i + x_0}{\sigma_0}\right)^2}, \tag{3}$$

which corresponds to two Gaussian peaks of FWHM σ_0 and centered around the abscissas x_0 and $-x_0$, respectively [Fig. 2(b)]. The relation between the parameters (x_0, σ_0) and (λ_x, σ_x) at depth y is determined by

$$x_0 = \frac{y \cdot \lambda_y}{\lambda_x} \tag{4}$$

and

$$\sigma_0 = \sqrt{2} \cdot \frac{y \cdot \lambda_y}{\sigma_x}. \tag{5}$$

2.B. Implementation

The implementation of the proposed unconventional beamforming strategy, devised to generate native RF-2D images in real-time, is realized on a research scanner (ultrasound advanced open platform, ULA-OP, Ref. 51), equipped with a linear array transducer composed of 128 elements.

2.B.1. Pseudodynamic focusing

According to the previously described dynamic focusing scheme, the gap in between the two Gaussian peaks is equal to $2x_0$ and is proportional to the depth y [Eq. (4)]. However, such an inverted "V" shape cannot be configured in the ULA-OP. Therefore, in order to match the conditions of the Fraunhofer approximation, the following scheme was adopted to implement the beamforming strategy on the scanner. Prior to the acquisition of a cine-loop for each subject, a first scan is performed only in the purpose to determine the depth y_0 corresponding to the rough location of the intima–media complex of the CCA far wall. Then, the constant value y_0 is used to configure the aperture function [Eqs. (4) and (5)]. The hypothesis that the aperture function can be approximated with a constant depth y_0 (i.e., with a "| |" shape) holds under the assumption that the assessed region of interest (ROI) remains at a pseudoconstant depth during the cine-loop. A previous study demonstrated that the average amplitude of the far wall motion along the axial direction in healthy subjects was 388 ± 198 μm.[14] Since the far wall is usually located at a depth y_0 corresponding roughly to 20 mm, such approximation has very little influence on the resulting spatial wavelength λ_x [Eq. (4)] and envelope σ_x [Eq. (5)].

2.B.2. Interleaving

In the scope of the present study, unconventional RF-2D images, as well as conventional RF images, are simultaneously acquired, by means of a so-called interleaving scheme. The purpose of this interleaving scheme is to generate a B-mode cine-loop from the RF signal subsequently to its acquisition, in order to enable human analysts to build a manual reference trajectory from a traditional clinical imaging modality. B-mode images provide visually understandable information about the imaged tissues and are typically generated via the application of a time gain compensation, a filtering, and an interpolation scheme onto the envelope of RF images. Interleaving consists in automatically alternating the configuration of the scanner, after each single image is acquired, between the unconventional (i.e., RF-2D) and conventional (i.e., RF) settings. After the entire cine-loop has been acquired and stored, the two distinct RF-2D and RF cine-loops are obtained by deinterleaving the stack of frames. Under the hypothesis that the frame rate is high enough w.r.t. the velocity of the tissues, it can be considered that both RF-2D and RF modalities represent the same information, namely, a quasi-identical region of the tissues is described by corresponding nth frames in both cine-loops. Finally, B-mode data are generated from the acquired RF data, by applying the Ultrasonix Amplio SDK (processing tool provided by Analogic Ultrasound, Boston, MA), which consists of RF-to-B conversion followed by speckle reduction.

2.B.3. Frame rate increase

Since images are acquired via the previously described interleaving scheme, the actual frame rate of both RF-2D and RF cine-loops is lowered by a factor two. In the aim to compensate for this effect and maintain a sufficiently high frame rate, only the first half of the transducer is activated (i.e., 64 elements out of 128), while the second half is disabled in both TX and RX phases. This strategy not only enables the

images to be acquired twice as fast but also implies that the width of the imaged region is reduced by half. Nevertheless, this trade-off is in good accordance with the aim of the present study, which is to assess the motion of a local region of the wall.

2.C. Local phase-based optical flow (LPBOF)

Subsequently to the acquisition and storage of the RF-2D images, motion tracking is performed offline by means of the previously introduced LPBOF estimator.[52,53] This approach aims at performing subpixel motion estimation by exploiting the phase information of the images. Briefly, the approach can be summarized as follows. Assume two ROIs, $\mathbf{I}_t$ and $\mathbf{I}_{t+1}$, from two consecutive RF-2D images of spatial frequencies (f_x,f_y) in a cine-loop. The aim is to estimate the 2D spatial displacement $(\hat{d}_x,\hat{d}_y)$, corresponding to the local optical flow from $\mathbf{I}_t$ to $\mathbf{I}_{t+1}$. First, two single-quadrant 2D analytic complex signals are extracted from the 2D Fourier spectrum of each ROI. Then, by calculating the phase of these analytic signals, and denoting $\overline{\phi}_1$ and $\overline{\phi}_2$ the mean differences between the corresponding phase signals of both ROIs, the spatial displacement $(\hat{d}_x,\hat{d}_y)$ is finally calculated as

$$\hat{d}_x = \frac{\overline{\phi}_1 - \overline{\phi}_2}{4\pi f_x},$$

$$\hat{d}_y = \frac{\overline{\phi}_1 + \overline{\phi}_2}{4\pi f_y}. \tag{6}$$

It is noteworthy that the spatial motion of the tissues is assessed without processing the spatial information (i.e., the pixel intensity) of the images. Instead, motion estimation is performed by the LPBOF estimator in the Fourier domain, by processing the phase information of the corresponding analytic signals.

2.D. Initialization

Motion tracking is performed in a semiautomated fashion by the LPBOF estimator. First, the user is required to select (one mouse click) a point in the first frame of the cine-loop, centered on the ROI to be tracked. Then, the motion of this point is automatically assessed through the entire cine-loop.

2.E. Collection of *in vivo* CCA cine-loops

Twenty-two young healthy volunteers (mean age 31 ± 6 yr, 14 males) as well as 6 elderly patients with high atherosclerosis risk (mean age 55 ± 17 yr, 6 females) were involved in the study. Five out of the six at-risk patients were diabetic. The only nondiabetic patient was 83 yr. Informed written consent was obtained from all participants. The study was conducted in compliance with the requirements of our institutional review board and the ethics committee. US image acquisition was performed by the same medical doctor, on both left and right CCAs, with a ULA-OP research scanner.[51] Subjects were scanned in the supine position, and performed a breath hold during the acquisition to avoid the influence of the movement due to breathing. The absence of atheromatous plaques in the imaged region was confirmed by a systematic visual inspection. Both RF-2D and conventional RF cine-loops were simultaneously acquired by means of interleaving, as described in Sec. 2.B.2. Images were recorded for a duration corresponding roughly to three consecutive cardiac cycles. The cine-loops were stored digitally and transferred to a commercial computer for off-line image analysis. For all participants, the cine-loop whose image quality was optimal among the left or right CCA was selected to be analyzed and the other one was discarded. Two healthy subjects were rejected from the study prior to image analysis due to poor image quality, namely, the intima–media complex of the far wall could not be clearly perceived on neither left nor right CCA. No patient was rejected from the study. The left CCA was selected to be analyzed in 3 participants among the 20 healthy volunteers and in 4 participants among the 6 at-risk patients.

2.F. Method evaluation

2.F.1. Trajectory reference

The tracking accuracy of the present method was evaluated for each assessed cine-loop. All analyses were conducted on the far wall of the CCA, to take advantage of a better echogenicity.[54] To quantify the performance of the tracking method despite the absence of ground truth inherent to *in vivo* imaging, reference trajectories were performed by three experienced analysts $\mathcal{A}_1$, $\mathcal{A}_2$, and $\mathcal{A}_3$. Analysts were specialists in US vascular imaging and processing, with 3, 6, and 12 yr of experience, respectively. The evaluation protocol, initially proposed in Ref. 14, can be summarized as follows. First, a single salient point, located within the intima–media complex of the far wall, was selected by the analyst $\mathcal{A}_1$ in the first frame of each cine-loop, as previously mentioned in Sec. 2.D. This initial selection was performed in the B-mode image representation. To allow each analyst to identify the same target in all remaining frames of the cine-loop, the selected point had to correspond to a well distinguishable echo scatterer and had to remain visible all along the cine-loop (Fig. 3).[13,14] Second, all analysts $\mathcal{A}_1$, $\mathcal{A}_2$, and $\mathcal{A}_3$ performed, independently from each others, the manual tracking of the set of initial points, during the complete duration of each cine-loop. These tracking operations were also performed in the B-mode image representation. A reference trajectory was subsequently generated by averaging, for each cine-loop, the three corresponding manual tracings. Intra-analyst variability was also assessed by the analyst $\mathcal{A}_2$ performing twice, for each cine-loop, the manual tracking operation. Third, the LPBOF method was applied onto the same set of initial points in the RF-2D image representation. The resulting trajectories obtained with the LPBOF estimator on RF-2D images were then evaluated against the reference tracings obtained manually on B-mode images.

2.F.2. Comparison with traditional speckle tracking

Aiming to assess the benefits of US-tagging for motion tracking, a traditional speckle tracking method,[55] also referred

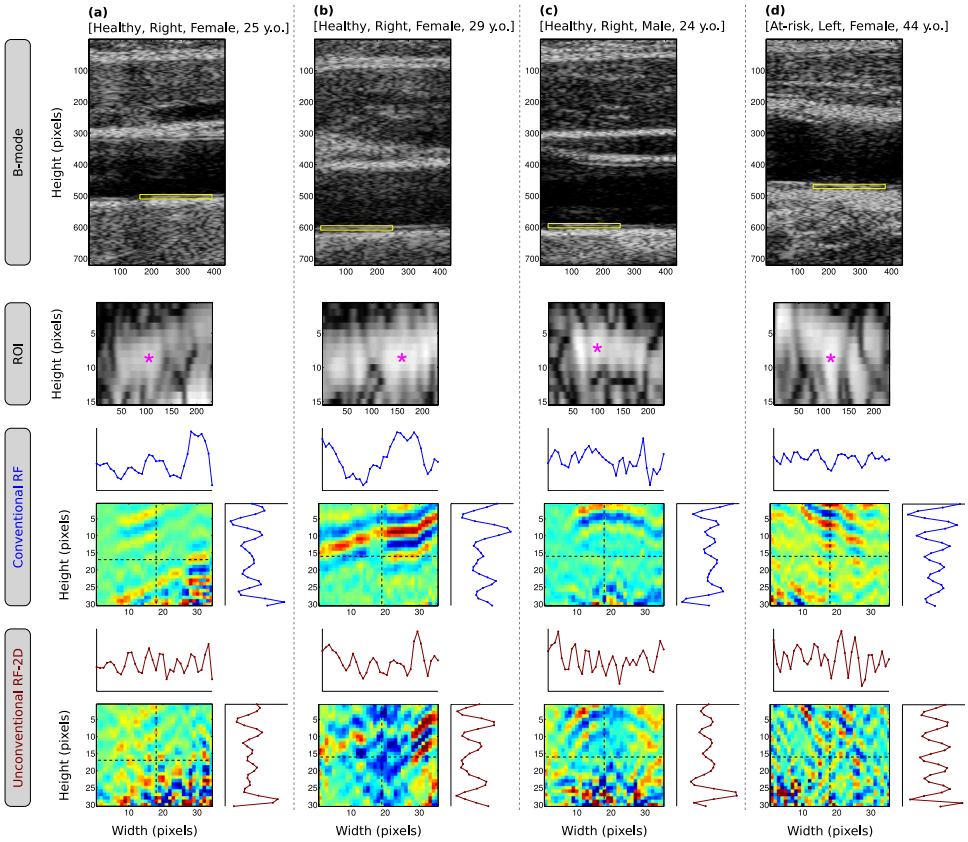

FIG. 3. Representative examples of resulting images of the common carotid artery, acquired *in vivo* in three healthy volunteers (a)–(c) and one at-risk patient (d). The cardiovascular status, carotid side, gender, and age are indicated for each subject. The B-mode images are displayed in the top row (15.62×28.12 mm^2). A ROI is located in the far wall and delimited by the yellow rectangle (8.30×0.57 mm^2). A zoomed view corresponding to this ROI is detailed, for different image modalities, in the second (B-mode, smooth blobby texture), third (RF, horizontal stripes), and fourth (RF-2D, chevron pattern) rows. In the B-mode zoomed ROI, the well distinguishable echo scatterer used by the analysts for manual tracking is indicated by the asterisk. In the RF and RF-2D zoomed ROIs, axial and longitudinal intensity profiles are depicted right to and above the images, respectively, and correspond to the location of the vertical and horizontal dashed lines, respectively. Along the axial profile, oscillations corresponding to the central frequency of the probe are present for both RF and RF-2D modalities. However, along the longitudinal profile, RF images do not abide to any specific pattern, whereas RF-2D images present a distinct periodic oscillations pattern. Let us recall that the spatial definition (i.e., pixel size) is not constant between the different image modalities, namely, 36×39 μm^2 for B-mode, and 245×19 μm^2 for RF and RF-2D. Therefore, the ROI size also differs, namely, 231×15 pixels vs 34×30 pixels.

to as block matching, was implemented for comparison. Conversely to the LPBOF estimator presented in this study, which is based on phase image information, the speckle tracking method is based on spatial image information, namely, the gray level of the pixels. Therefore, the speckle tracking method was applied on conventional US images, rather than on unconventional RF-2D images whose specificity is to provide a 2D frequency carrier for phase-based methods. Although B-mode images were reconstructed from conventional RF signals in the objective to allow human observers to perform the manual tracking of the tissues, as previously detailed in Secs. 2.B.2 and 2.F.1, the quality of such in-house B-mode images remains suboptimal w.r.t. common standards provided by commercial clinical scanners. Therefore, the speckle tracking method was applied to the envelope of the conventional RF images rather than to the B-mode images. Tracking was performed onto the same set of initial points followed by the three analysts. The similarity criterion used in this implementation was the normalized sum of squared differences. The resulting trajectories obtained with speckle tracking on the envelope of RF images were then evaluated against the reference tracings obtained manually on B-mode images.

2.G. Parameters settings

The present framework was applied with the following parameters settings. The central frequency f_y of the probe was 4 MHz, the sampling frequency was 50 MHz, and the dynamic range was 65 dB. The penetration depth was 28.5 mm, and the width of the imaged region was 15.7 mm. The longitudinal and axial dimensions of the RF-2D and RF images were 64×1500 pixel, with a pixel size of 245×19 μm^2. The longitudinal and axial dimensions of the B-mode images were 434×721 pixel, with a pixel size of 36×39 μm^2. Images were recorded for a duration of 3.28 s at the frame rate of 183 fps, yielding two deinterleaved cine-loops (i.e., RF-2D and RF images) whose actual frame rate was 91 fps and whose total number of frames was 300. The frame rate of the B-mode images, reconstructed from the RF images, also corresponded to 91 fps.

Aiming to generate RF-2D images whose longitudinal wavelength λ_x corresponds to 1.20 mm and whose envelope FWHM σ_x corresponds to 2.90 mm, the two Gaussian peaks of the aperture function were defined by the FWHM σ_0 equal to 0.98 mm [Eq. (4)] and the abscissa x_0 equal to 2.45 mm [Eq. (5)]. Motion tracking with the LPBOF estimator was performed with a ROI size of 2.45×0.30 mm^2 (i.e., encompassing two wavelengths of oscillations in both longitudinal and axial directions). The traditional speckle tracking method was applied with the following empirically determined parameters settings: block size of 1.47×0.23 mm^2, and search-window size of 1.72×0.34 mm^2.

2.H. Statistical analysis

The Mann–Whitney U test was used to compare the tracking errors between LPBOF and traditional speckle tracking, as well as the values of LOKI amplitude ΔX between healthy volunteers and elderly patients. The value $p < 0.05$ was considered to indicate a statistically significant difference. Statistical analysis was performed using MATLAB (MATLAB 7.14, The MathWorks, Inc., Natick, MA, 2011).

3. RESULTS

RF-2D cine-loops of the CCA were acquired by means of the previously described US-tagging beamforming strategy. Resulting examples of *in vivo* RF-2D images, featuring oscillations in both axial and longitudinal profiles, are depicted in Fig. 3. Along the axial profile, the spatial wavelength of the oscillations, determined by the central frequency f_y of the transducer, corresponded to 152 μm. Along the longitudinal profile, the spatial wavelength of the oscillations, determined by the aperture function [Fig. 2, Eqs. (4) and (5)], corresponded to 1470 μm. A clear difference can be observed between the RF and RF-2D images displayed in Fig. 3: RF images are characterized by a horizontally striped pattern, caused by the reflection of the beam with the intima and media layers, whereas RF-2D images are characterized by a checkerboard-like pattern, caused by interference between axial and transverse oscillations.

As previously described, the motion of the intima–media complex was assessed on a single local salient point for each subject. Tracking was performed in RF-2D cine-loops by the LPBOF estimator, as well as in B-mode cine-loops by the analysts $\mathcal{A}_1$, $\mathcal{A}_2$, and $\mathcal{A}_3$. A comparison with a traditional speckle tracking method was also realized, by tracking the same set of points in the envelope of RF cine-loops. The tracking error was defined as the absolute difference between the estimated coordinates of the tracked point and the corresponding reference, in each individual frame, for both axial and longitudinal directions. The average absolute tracking error of both semiautomated tracking methods w.r.t. the reference trajectory for each analyzed subject is indicated in Table I, alongside the inter- and intra-analysts variability. The difference between the mean absolute tracking errors of LPBOF and traditional speckle tracking was statistically significant in the longitudinal direction ($p = 9\times10^{-7}$), but not in the axial direction ($p = 0.3275$). The trajectories estimated with the present method were close to the corresponding reference, as depicted in Fig. 4.

TABLE I. Average absolute tracking errors (μm).

Errors	Longitudinal	Axial
Healthy volunteers (n = 20)		
LPBOF vs reference	99 ± 86	57 ± 45
Speckle tracking vs reference	278 ± 247	62 ± 51
Interanalysts variability	141 ± 125	74 ± 67
Intra-analysts variability	141 ± 154	39 ± 54
At-risk patients (n = 6)		
LPBOF vs reference	95 ± 76	46 ± 36
Speckle tracking vs reference	332 ± 310	67 ± 54
Interanalysts variability	104 ± 91	66 ± 61
Intra-analysts variability	98 ± 81	36 ± 46
All (n = 26)		
LPBOF vs reference	98 ± 84	55 ± 44
Speckle tracking vs reference	291 ± 264	63 ± 51
Interanalysts variability	133 ± 119	72 ± 66
Intra-analysts variability	131 ± 142	38 ± 52

When analyzing these errors, it is also insightful to compare them with the actual amplitude of the tissues motion. We define ΔX and ΔY as the peak-to-peak motion amplitude derived from the longitudinal and axial trajectories, respectively [Fig. 4(a)]. For all the 26 assessed participants, the mean values of the longitudinal and axial motion amplitudes corresponded to 444 ± 210 μm and 470 ± 173 μm, respectively. More specifically, the mean longitudinal and axial motion amplitudes were 486 ± 211 μm and 528 ± 129 μm for the 20 healthy volunteers, and 302 ± 147 μm and 278 ± 171 μm for the 6 elderly patients, respectively. Calculating the ratios between the absolute tracking errors of each cine-loop and the corresponding longitudinal and axial amplitudes, the mean longitudinal and axial relative error values were $28\%\pm23\%$ of ΔX and $13\%\pm9\%$ of ΔY for all the assessed participants, $23\%\pm11\%$ of ΔX and $11\%\pm4\%$ of ΔY for the healthy volunteers, and $47\%\pm41\%$ of ΔX and $21\%\pm15\%$ of ΔY for the elderly patients, respectively.

LOKI amplitude ΔX was reduced in elderly patients ($\Delta X = 486\pm211$ μm) w.r.t. healthy volunteers ($\Delta X = 302\pm147$ μm), as displayed in Fig. 5. This is in accordance with previous studies.[7–11] However, the difference between the two populations was not statistically significant ($p = 0.0828$). Let us note that the axial amplitude ΔY of the far wall itself is not relevant as it does not represent the cross-sectional diameter change. Therefore, no statistical comparison of this parameter between the two populations was conducted.

4. DISCUSSION AND CONCLUSIONS

A framework dedicated to assess tissue motion in tagged US images was introduced. The two main contributions of the present study are (i) the implementation of an unconventional

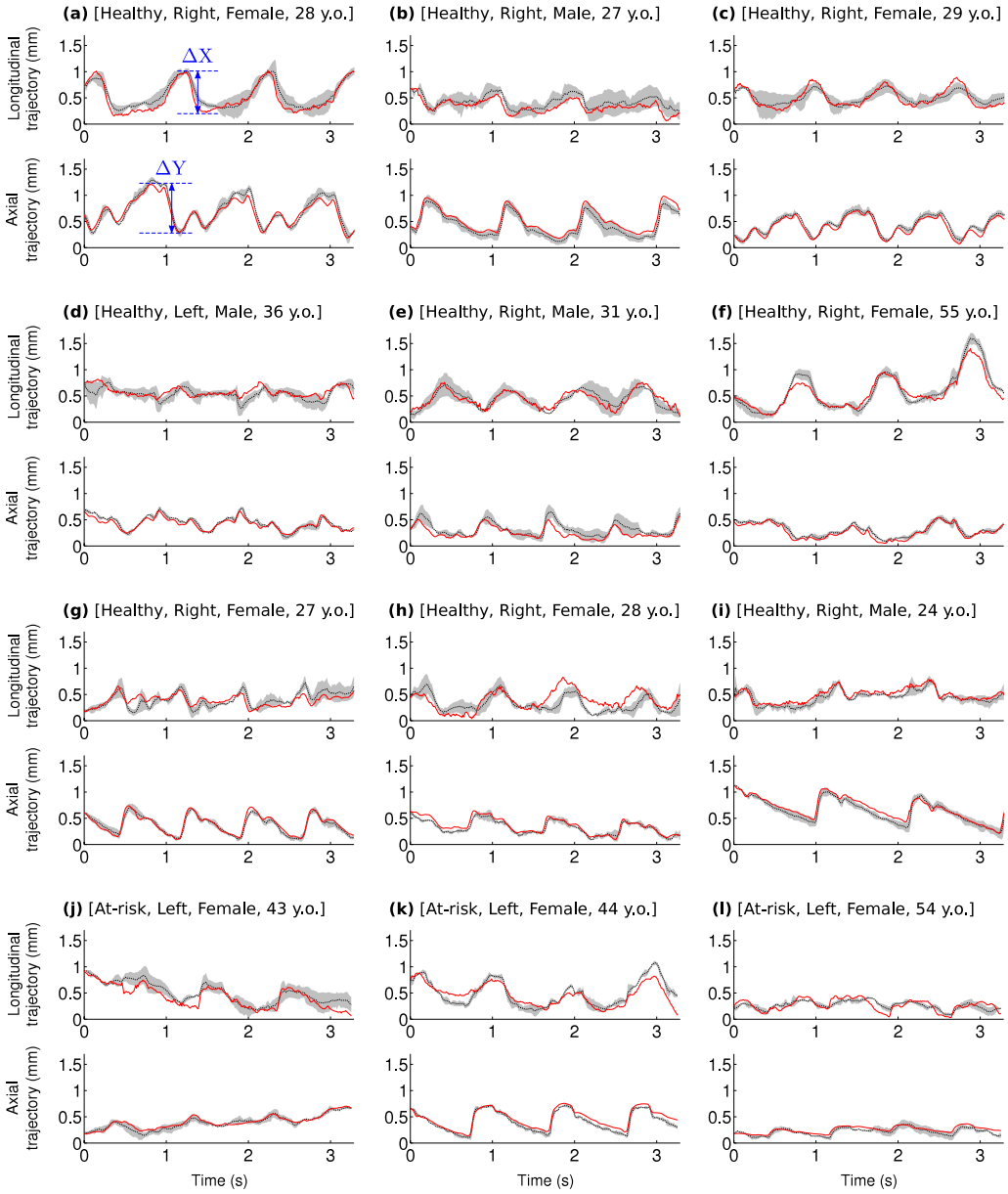

FIG. 4. Representative examples of the periodic tissues motion over several cardiac cycles, evaluated in nine healthy volunteers (a)–(i) and three at-risk patients (j)–(l), in both longitudinal and axial directions. The red solid line, black dotted line, and gray area represent the result of the semiautomatic LPBOF tracking method, the reference trajectory calculated as the averaged tracings performed manually by three analysts, and the standard deviation of the three manual tracings, respectively. The cardiovascular status, carotid side, gender, and age are indicated for each subject. Schematic representation the motion amplitude ΔX and ΔY is displayed in (a).

beamforming strategy on a US scanner, devised to acquire native RF-2D images in real-time, and (ii) the *in vivo* application of US-tagging to track the CCA wall motion during consecutive cardiac cycles, by means of a specific phase-based estimator. Twenty young healthy volunteers and six elderly patients were involved in this study. Results demonstrate that this framework is well suited to evaluate LOKI (i.e., the cyclic shearing motion of the intima–media complex over the tunica adventitia along the direction parallel to the blood flow), which represents a clinically relevant yet challenging to assess pathophysiological parameter.[14]

The evaluation of the proposed tracking framework was conducted *in vivo* onto 20 healthy volunteers and 6 at-risk patients, against reference trajectories manually generated by 3 experts analysts. In this purpose, RF signals were simultaneously acquired alongside RF-2D signals by means of an interleaving scheme and used to reconstruct B-mode cine-loops, i.e., images that are visually understandable and where motion can reliably be tracked by human analysts. A performance comparison was also realized with a traditional speckle tracking method on the envelope of the RF cine-loops. When analyzing the results, the tracking accuracy of the LPBOF estimator was nearly three times higher than the accuracy of the speckle tracking method along the longitudinal direction, whereas the accuracy of both approaches was similar along the axial direction (Table I).

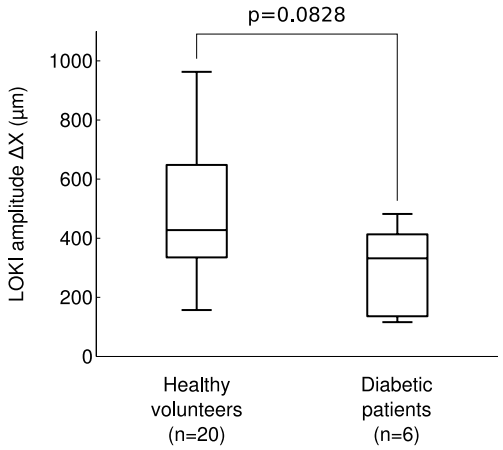

FIG. 5. Box plot representing LOKI amplitude ΔX, for healthy volunteers and elderly patients. Percentiles are indicated by boxes (25th and 75th), inner lines (50th) and error bars (5th and 95th). The result of the Mann–Whitney U test is indicated by the p value.

This demonstrates that the introduction of TOs in the images contributes to improve the estimation of the longitudinal component of the motion. The rather large standard deviation of the average absolute tracking errors testifies of the presence of challenging cases in our dataset. In the present study, the tracking error realized by the LPBOF method along the longitudinal direction was roughly twice larger than the error along the axial direction (Table I). This phenomenon was also observed for the inter- and intravariability of the manual tracings. This is in accordance with the results of previously introduced tracking methods, which also demonstrated a greater inaccuracy along the longitudinal direction.[14]

When comparing the tracking performance of the present framework, for both longitudinal and axial directions, results demonstrated that the mean *absolute* errors were similar between healthy volunteers and at-risk patients, as presented in Table I. However, since the motion amplitude was reduced in at-risk participants ($\Delta X = 302 \pm 147$ μm and $\Delta Y = 278 \pm 171$ μm) w.r.t. healthy controls ($\Delta X = 486 \pm 211$ μm and $\Delta Y = 528 \pm 129$ μm), the tracking errors relative to the motion amplitude were larger in at-risk participants compared to healthy controls. Indeed, the mean *relative* errors were approximately twice higher in elderly patients ($47\% \pm 41\%$ of ΔX and $21\% \pm 15\%$ of ΔY) w.r.t. healthy volunteers ($23\% \pm 11\%$ of ΔX and $11\% \pm 4\%$ of ΔY). These results suggest that the overall performances of the present framework decrease when the total motion amplitude becomes smaller. A similar trend has been reported in previous work using conventional B-mode.[14]

The quality of the in-house reconstructed B-mode images was sufficient for the three analysts to manually track the wall motion during the cardiac cycle. However, such quality remained suboptimal w.r.t. common standards provided by commercial clinical scanners. For this reason, semiautomated state-of-the-art tracking methods were not applied to the B-mode cine-loops for further performance comparison with the present framework, as it is likely that the results would have been negatively biased. Nevertheless, six different state-of-the-art tracking methods have previously been evaluated in a dataset of 81 B-mode cine-loops of the CCA routinely acquired with a clinical scanner (Antares, Siemens, Erlangen, Germany).[14] Although the pertinence of such comparison is limited by the fact that the set of analyzed subjects was different, the present framework would rank, among all these methods, second for the estimation of the longitudinal trajectory and third for the estimation of the axial trajectory.

Particular care must be taken when designing the probe aperture function (Fig. 2). First, the FWHM σ_0 of the two Gaussian peaks determines the number of activated elements in the RX phase but also impacts on the FWHM σ_x of the signal envelope within the tissues [Eq. (5)]. Thus, a large σ_0 value would enable the image to be acquired with more energy but would also result in a small σ_x value and yield a narrow signal envelope that would not encompass the wavelength λ_x of the oscillations. Conversely, a broad signal envelope σ_x would permit the TOs to be visualized over several wavelengths, but would require a small σ_0 value, and the transmitted energy would thus potentially be insufficient to image the tissues. Second, the parameter x_0 defines the gap between the two Gaussian peaks and also determines the spatial wavelength λ_x of the TOs [Eq. (4)]. A small x_0 value would result in a large wavelength λ_x. This would be likely to decrease the tracking accuracy, since a larger encompassing ROI would be required to extract the phase information and estimate the motion. Conversely, a large x_0 value would yield a small wavelength λ_x. In this case, tracking accuracy would also be compromised as the oscillations would not be perceptible if their wavelength is inferior to two pixels. Additionally, small as well as large values of x_0 would also both necessitate σ_0 to be small in order to represent an aperture function consisting of two Gaussian peaks, each fully represented by half of the elements of the probe. In the present implementation of the unconventional aperture function, the value of each parameter was determined to optimize the image acquisition, as detailed in Sec. 2.G.

The clinical motivation of the present work lies in the detection of very early stage atherosclerosis. Indeed, as the syndrome follows a complex evolution with an important proportion of events occurring without premonitory signs,[56] early risk prediction in asymptomatic populations (i.e., prior to plaque formation) toward an appropriate prevention strategy represents a major public health issue.[57–59] Yet, the screening potential of traditional risk markers (e.g., PWV, IMT) remains limited, as they demonstrate a fair or poor overall strength of evidence and lack applicability.[3,60,61] However, in recent studies, compelling evidence showed that LOKI constitutes a solid candidate to become a valuable image-based biomarker for cardiovascular disease, as it is associated with the presence of cardiovascular risk factors[7–10] and with the occurrence of clinical events.[11] Moreover, LOKI-induced forces are likely to be associated with wall shear strain, which is a key factor in the development of atherosclerosis and plays a crucial role in vasa vasorum circulation as well as endothelial function.[62,63] These findings strongly suggest that LOKI-screening may improve cardiovascular risk stratification in patients with subclinical atherosclerosis.

In this study, healthy volunteers and elderly patients at high atherosclerosis risk were involved. Results showed that LOKI amplitude ΔX was reduced in at-risk patients w.r.t. healthy volunteers ($\Delta X = 486 \pm 211$ μm vs $\Delta X = 302 \pm 147$ μm, $p = 0.0828$), which is in accordance with previous work,[7–11] and putatively suggest that the arterial wall of at-risk patients is stiffer. Five out of the six elderly patients were diabetic. However, since the two populations were not age-matched, the influence of diabetes *per se* could not be assessed. Let us also note that, when comparing ΔX between the two populations, no statistical difference was found. To address these two points, future investigations will be conducted, involving larger populations of age-matched participants.

A limitation of the present framework consists in its application to a rather narrow and heterogeneous region, namely, the intima–media complex of the arterial wall (Fig. 1). The successive impedance transitions between the lumen–intima and media–adventitia indeed contribute to generate a pressure field that could potentially influence TOs formation. Accordingly, further studies will investigate this effect, by involving patients whose IMT is thicker, as well as patients with heterogeneous atherosclerotic plaques. Future perspectives also include the combination of US-tagging with ultrafast imaging (i.e., up to 10 000 fps) to assess the progressive attenuation of the LOKI-inducing forces within the tissues from the heart to the head.[64]

In conclusion, an unconventional beamforming scheme dedicated to acquire tagged US images in real-time was introduced. The rationale of such approach is to improve the estimation of the longitudinal component of the motion by embedding a distinct pattern along the longitudinal profile of the image. The present framework was applied *in vivo* to acquire RF-2D cine-loops of the common carotid artery in healthy volunteers and at-risk patients. Tracking performances demonstrate that US-tagging represents a promising technique to improve motion tracking in clinical applications.

ACKNOWLEDGMENTS

The authors would like to thank Mrs. Adeline Bernard for her skillful technical assistance. This work was done within the French ANR LABEX PRIMES (ANR-11-LABX-0063) and CeLyA (ANR-10-LABX-0060) of Université de Lyon, within the program "Investissements d'Avenir" (ANR-11-IDEX-0007) operated by the French National Research Agency (ANR).

[a]Author to whom correspondence should be addressed. Electronic mail: g.zahnd@erasmusmc.nl

[1]World Health Organization, Cardiovascular diseases (CVDs), Fact sheet number 317, http://www.who.int/mediacentre/factsheets/fs317/en/index.html, March 2013.

[2]S. Laurent, J. Cockcroft, L. Van Bortel, P. Boutouyrie, C. Giannattasio, D. Hayoz, B. Pannier, C. Vlachopoulos, I. Wilkinson, and H. Struijker-Boudier, "Expert consensus document on arterial stiffness: Methodological issues and clinical applications," Eur. Heart J. **27**(21), 2588–2605 (2006).

[3]A. Simon, G. Chironi, and J. Levenson, "Performance of subclinical arterial disease detection as a screening test for coronary heart disease," Hypertension **48**(3), 392–396 (2006).

[4]M. Persson, Å. R. Ahlgren, T. Jansson, A. Eriksson, H. W. Persson, and K. Lindström, "A new non-invasive ultrasonic method for simultaneous measurements of longitudinal and radial arterial wall movements: First in vivo trial," Clin. Physiol. Funct. Imaging **23**(5), 247–251 (2003).

[5]M. Cinthio, Å. R. Ahlgren, J. Bergkvist, T. Jansson, H. W. Persson, and K. Lindström, "Longitudinal movements and resulting shear strain of the arterial wall," Am. J. Physiol. **291**(1), H394–H402 (2006).

[6]T. Idzenga, S. Holewijn, H. H. G. Hansen, and C. L. de Korte, "Estimating cyclic shear strain in the common carotid artery using radiofrequency ultrasound," Ultrasound Med. Biol. **38**(12), 2229–2237 (2012).

[7]Å. R. Ahlgren, M. Cinthio, S. Steen, H. W. Persson, T. Sjöberg, and K. Lindström, "Effects of adrenaline on longitudinal arterial wall movements and resulting intramural shear strain: A first report," Clin. Physiol. Funct. Imaging **29**(5), 353–359 (2009).

[8]G. Zahnd, L. Boussel, A. Marion, M. Durand, P. Moulin, A. Sérusclat, and D. Vray, "Measurement of two-dimensional movement parameters of the carotid artery wall for early detection of arteriosclerosis: A preliminary clinical study," Ultrasound Med. Biol. **37**(9), 1421–1429 (2011).

[9]G. Zahnd, D. Vray, A. Sérusclat, D. Alibay, M. Bartold, A. Brown, M. Durand, L. M. Jamieson, K. Kapellas, L. J. Maple-Brown, K. O'Dea, P. Moulin, D. S. Celermajer, and M. R. Skilton, "Longitudinal displacement of the carotid wall and cardiovascular risk factors: Associations with aging, adiposity, blood pressure and periodontal disease independent of cross-sectional distensibility and intima-media thickness," Ultrasound Med. Biol. **38**(10), 1705–1715 (2012).

[10]Å. R. Ahlgren, M. Cinthio, S. Steen, T. Nilsson, T. Sjöberg, H. W. Persson, and K. Lindström, "Longitudinal displacement and intramural shear strain of the porcine carotid artery undergo profound changes in response to catecholamines," Am. J. Physiol.: Heart Circ. Physiol. **302**(5), H1102–H1115 (2012).

[11]S. Svedlund, C. Eklund, P. Robertsson, M. Lomsky, and L. M. Gan, "Carotid artery longitudinal displacement predicts 1-year cardiovascular outcome in patients with suspected coronary artery disease," Arterioscler., Thromb., Vasc. Biol. **31**(7), 1668–1674 (2011).

[12]S. Golemati, A. Sassano, M. J. Lever, A. A. Bharath, S. Dhanjil, and A. N. Nicolaides, "Carotid artery wall motion estimated from B-mode ultrasound using region tracking and block matching," Ultrasound Med. Biol. **29**(3), 387–399 (2003).

[13]M. Cinthio, Å. R. Ahlgren, T. Jansson, A. Eriksson, H. W. Persson, and K. Lindström, "Evaluation of an ultrasonic echo-tracking method for measurements of arterial wall movements in two dimensions," IEEE Trans. Ultrason., Ferroelectrics, Freq. Control **52**(8), 1300–1311 (2005).

[14]G. Zahnd, M. Orkisz, A. Sérusclat, P. Moulin, and D. Vray, "Evaluation of a Kalman-based block matching method to assess the bi-dimensional motion of the carotid artery wall in B-mode ultrasound sequences," Med. Image Anal. **17**(5), 573–585 (2013).

[15]A. Gastounioti, S. Golemati, J. S. Stoitsis, and K. S. Nikita, "Carotid artery wall motion analysis from B-mode ultrasound using adaptive block matching: In silico evaluation and in vivo application," Phys. Med. Biol. **58**(24), 8647–8661 (2013).

[16]T. Numata, H. Hasegawa, and H. Kanai, "Basic study on detection of outer boundary of arterial wall using its longitudinal motion," Jpn. J. Appl. Phys. Part 1 **46**(7B), 4900–4907 (2007).

[17]C. Sumi, "Fine elasticity imaging utilizing the iterative RF-echo phase matching method," IEEE Trans. Ultrason., Ferroelectrics, Freq. Control **46**(1), 158–166 (1999).

[18]A. Pesavento, C. Perrey, M. Krueger, and H. Ermert, "A time-efficient and accurate strain estimation concept for ultrasonic elastography using iterative phase zero estimation," IEEE Trans. Ultrason., Ferroelectrics, Freq. Control **46**(5), 1057–1067 (1999).

[19]X. Chen, M. J. Zohdy, S. Y. Emelianov, and M. O'Donnell, "Lateral speckle tracking using synthetic lateral phase," IEEE Trans. Ultrason., Ferroelectrics, Freq. Control **51**(5), 540–550 (2004).

[20]E. S. Ebbini, "Phase-coupled two-dimensional speckle tracking algorithm," IEEE Trans. Ultrason., Ferroelectrics, Freq. Control **53**(5), 972–990 (2006).

[21]Y. Wan, D. Liu, and E. S. Ebbini, "Simultaneous imaging of tissue motion and flow velocity using 2D phase-coupled speckle tracking," in *IEEE International Ultrasonics Symposium* (New York, NY, 2010), pp. 487–490.

[22]T. Maltaverne, P. Delachartre, and A. Basarab, "Motion estimation using the monogenic signal applied to ultrasound elastography," in *IEEE Engineering in Medicine and Biology Society* (2010), pp. 33–36.

[23]M. Alessandrini, H. Liebgott, A. Basarab, P. Clarysse, and O. Bernard, "Monogenic signal for cardiac motion analysis from tagged magnetic resonance image sequences," in *Computing in Cardiology* (2012), pp. 685–688.
[24]R. Abbal, A. Basarab, and D. Kouame, "3D translation estimation using the monogenic orientation vector," in *IEEE International Symposium on Biomedical Imaging* (2012), pp. 1591–1594.
[25]M. Alessandrini, H. Liebgott, and O. Bernard, "Monogenic phase based optical flow computation for myocardial motion analysis in 3D echocardiography," in *Medical Image Computing and Computer Assisted Intervention* (Springer-Verlag, Berlin, 2012), pp. 159–168.
[26]J. A. Jensen and P. Munk, "A new method for estimation of velocity vectors," IEEE Trans. Ultrason., Ferroelectrics, Freq. Control **45**(3), 837–851 (1998).
[27]M. E. Aderson, "Multi-dimensional velocity estimation with ultrasound using spatial quadrature," IEEE Trans. Ultrason., Ferroelectrics, Freq. Control **45**(3), 852–861 (1998).
[28]J. Udesen and J. A. Jensen, "Investigation of transverse oscillation method," IEEE Trans. Ultrason., Ferroelectrics, Freq. Control **53**(5), 959–971 (2006).
[29]K. L. Hansen, J. Udesen, C. Thomsen, J. A. Jensen, and M. B. Nielsen, "Validation of transverse oscillation vector velocity estimation in-vivo," in *IEEE International Ultrasonics Symposium* (New York, NY, 2007), pp. 1093–1096.
[30]K. Hansen, J. Udesen, C. Thomsen, J. A. Jensen, and M. Nielsen, "In vivo validation of a blood vector velocity estimator with MR angiography," IEEE Trans. Ultrason., Ferroelectrics, Freq. Control **56**(1), 91–100 (2009).
[31]J. A. Jensen, "Spectral velocity estimation in the transverse direction," in *IEEE International Ultrasonics Symposium* (New York, NY, 2013), pp. 631–634.
[32]J. A. Jensen, S. Nikolov, J. Udesen, P. Munk, K. L. Hansen, M. M. Pedersen, P. M. Hansen, M. B. Nielsen, N. Oddershede, J. Kortbek, M. J. Pihl, Y., and Li, "Recent advances in blood vector velocity imaging," in *IEEE International Ultrasonics Symposium* (New York, NY, 2011).
[33]M. J. Pihl and J. A. Jensen, "3D vector velocity estimation using a 2D phased array," in *IEEE International Ultrasonics Symposium* (New York, NY, 2012), pp. 1881–1885.
[34]S. Salles, H. Liebgott, D. Garcia, and D. Vray, "Real time 3D US-tagging combined with 3D phase-based motion estimation," in *IEEE International Ultrasonics Symposium* (New York, NY, 2013), pp. 585–588.
[35]H. Liebgott, J. Fromageau, J. E. Wilhjelm, D. Vray, and P. Delachartre, "Beamforming scheme for 2D displacement estimation in ultrasound imaging," EURASIP J. Adv. Signal Process. **8**, 1212–1220 (2005).
[36]H. Liebgott, J. E. Wilhjelm, J. A. Jensen, D. Vray, and P. Delachartre, "PSF dedicated to estimation of displacement vectors for tissue elasticity imaging with ultrasound," IEEE Trans. Ultrason., Ferroelectrics, Freq. Control **54**(4), 746–756 (2007).
[37]C. Sumi, T. Noro, and A. Tanuma, "Effective lateral modulations with applications to shear modulus reconstruction using displacement vector measurement," IEEE Trans. Ultrason., Ferroelectrics, Freq. Control **55**(12), 2607–2625 (2008).
[38]G. Zahnd, A. Basarab, H. Liebgott, O. Basset, and P. Delachartre, "Real-time specific beamforming applied to motion trajectory estimation in ultrasound imaging," in *IEEE International Ultrasonics Symposium* (New York, NY, 2009), pp. 1342–1345.
[39]H. Liebgott, A. Basarab, S. Marincas, O. Bernard, and D. Friboulet, "Tangential oscillations for motion estimation in echocardiography," in *IEEE International Ultrasonics Symposium* (New York, NY, 2008), pp. 1761–1764.
[40]H. Liebgott, A. Ben Salem, A. Basarab, H. Gao, P. Claus, J. D'hooge, P. Delachartre, and D. Friboulet, "Tangential sound field oscillations for 2D motion estimation in echocardiography," in *IEEE International Ultrasonics Symposium* (New York, NY, 2009), pp. 498–501.
[41]M. Alessandrini, A. Basarab, L. Boussel, X. Guo, A. Serusclat, D. Friboulet, D. Kouamé, O. Bernard, and H. Liebgott, "A new technique for the estimation of cardiac motion in echocardiography based on transverse oscillations: A preliminary evaluation in silico and a feasibility demonstration in vivo," IEEE Trans. Med. Imaging **33**(5), 1148–1162 (2014).
[42]M. Alessandrini, H. Liebgott, D. Friboulet, and O. Bernard, "Monogenic phase based myocardium motion analysis from cardiac ultrasound with transverse oscillations," in *IEEE International Ultrasonic Symposium* (New York, NY, 2012), pp. 1098–1101.
[43]M. Alessandrini, A. Basarab, H. Liebgott, and O. Bernard, "Myocardial motion estimation from medical images using the monogenic signal," IEEE Trans. Image Process. **22**(3), 1084–1095 (2013).
[44]X. Guo, D. Friboulet, and H. Liebgott, "Transverse oscillations beamformer design for sector scan using back-propagation," in *IEEE International Symposium on Biomedical Imaging* (New York, NY, 2012), pp. 1100–1103.
[45]J. A. Jensen, "Optimization of transverse oscillating fields for vector velocity estimation with convex arrays," in *IEEE International Ultrasonics Symposium* (New York, NY, 2013), pp. 1753–1756.
[46]S. Salles, G. Zahnd, H. Liebgott, A. Sérusclat, and D. Vray, "Real time US-tagging combined with phase-based optical flow applied to 2D motion estimation of the carotid artery wall," in *IEEE International Ultrasonics Symposium* (New York, NY, 2012), pp. 1185–1188.
[47]S. Salles, D. Garcia, B. Bou-Saïd, F. Savary, A. Sérusclat, D. Vray, and H. Liebgott, "Plane wave transverse oscillation (PWTO): An ultra-fast transverse oscillation imaging mode performed in the Fourier domain for 2D motion estimation of the carotid artery," in *IEEE International Symposium on Biomedical Imaging* (2014), pp. 1409–1412.
[48]G. R. Lockwood, J. R. Talman, and S. S. Brunke, "Real-time 3-D ultrasound imaging using sparse synthetic aperture beamforming," IEEE Trans. Ultrason., Ferroelectrics, Freq. Control **45**(4), 980–988 (1998).
[49]H. Liebgott, A. Basarab, P. Gueth, C. Cachard, and P. Delachartre, "Lateral RF image synthesis using a synthetic aperture imaging technique," IEEE Trans. Ultrason., Ferroelectrics, Freq. Control **55**(9), 2097–2103 (2008).
[50]J. W. Goodman and E. M. Cox, "Introduction to fourier optics," Phys. Today **22**(4), 97–101 (1969).
[51]P. Tortoli, L. Bassi, E. Boni, A. Dallai, F. Guidi, and S. Ricci, "ULA-OP: An advanced open platform for ultrasound research," IEEE Trans. Ultrason., Ferroelectrics, Freq. Control **56**(10), 2207–2216 (2009).
[52]A. Basarab, P. Gueth, H. Liebgott, and P. Delachartre, "Phase-based block matching applied to motion estimation with unconventional beamforming strategies," IEEE Trans. Ultrason., Ferroelectrics, Freq. Control **56**(5), 945–957 (2009).
[53]A. Basarab, H. Liebgott, and P. Delachartre, "Analytic estimation of subsample spatial shift using the phases of multidimensional analytic signals," IEEE Trans. Image Process. **18**(2), 440–447 (2009).
[54]J. Wikstrand, "Methodological considerations of ultrasound measurement of carotid artery intima-media thickness and lumen diameter," Clin. Physiol. Funct. Imaging **27**(6), 341–345 (2007).
[55]L. Bohs and G. Trahey, "A novel method for angle independent ultrasonic imaging of blood flow and tissue motion," IEEE Trans. Biomed. Eng. **38**(3), 280–286 (1991).
[56]C. Napoli, L. O. Lerman, F. de Nigris, M. Gossl, M. L. Balestrieri, and A. Lerman, "Rethinking primary prevention of atherosclerosis-related diseases," Circulation **114**(23), 2517–2527 (2006).
[57]S. N. Pearson *et al.*, "AHA guidelines for primary prevention of cardiovascular disease and stroke: 2002 update consensus panel guide to comprehensive risk reduction for adult patients without coronary or other atherosclerotic vascular diseases," Circulation **106**(3), 388–391 (2002).
[58]E. S. Ford, U. A. Ajani, J. B. Croft, J. A. Critchley, D. R. Labarthe, T. E. Kottke, W. H. Giles, and S. Capewell, "Explaining the decrease in US deaths from coronary disease, 1980–2000," New Engl. J. Med. **356**(23), 2388–2398 (2007).
[59]P. Greenland *et al.*, "2010 ACCF/AHA guideline for assessment of cardiovascular risk in asymptomatic adults," J. Am. Coll. Cardiol. **56**(25), e50–e103 (2010).
[60]M. Helfand, D. I. Buckley, M. Freeman, R. Fu, K. Rogers, C. Fleming, and L. L. Humphrey, "Emerging risk factors for coronary heart disease: A summary of systematic reviews conducted for the U.S. Preventive Services Task Force," Ann. Intern. Med. **151**(7), 496–507 (2009).
[61]M. W. Lorenz *et al.*, "Carotid intima-media thickness progression to predict cardiovascular events in the general population (the PROG-IMT collaborative project): A meta-analysis of individual participant data," Lancet **379**(9831), 2053–2062 (2012).
[62]K. S. Cunningham and A. I. Gotlieb, "The role of shear stress in the pathogenesis of atherosclerosis," Lab. Invest. **85**(1), 9–23 (2004).
[63]Y. S. Chatzizisis, A. U. Coskun, M. Jonas, E. R. Edelman, C. L. Feldman, and P. H. Stone, "Role of endothelial shear stress in the natural history of coronary atherosclerosis and vascular remodeling: Molecular, cellular, and vascular behavior," J. Am. Coll. Cardiol. **49**(25), 2379–2393 (2007).
[64]G. Zahnd, S. Balocco, A. Sérusclat, P. Moulin, M. Orkisz, and D. Vray, "Progressive attenuation of the longitudinal kinetics in the common carotid artery: Preliminary in vivo assessment," Ultrasound Med. Biol. **41**(1), 339–345 (2015).